The Role of Neutral Singular Vectors in Midlatitude Air–Sea Coupling

JASON C. GOODMAN* AND JOHN MARSHALL

Program in Atmospheres, Oceans, and Climate, Department of Earth, Atmospheric, and Planetary Sciences, Massachusetts Institute of Technology, Cambridge, Massachusetts

(Manuscript received 21 June 2001, in final form 4 March 2002)

ABSTRACT

The role of ''neutral vectors'' in midlatitude air–sea interaction is studied in a simple coupled model. Neutral vectors—the right singular vectors of the linearized atmospheric model tendency matrix with the smallest singular values—are shown to act as pattern-specific amplifiers of ocean SST anomalies and dominate coupled behavior.

These ideas are developed in the framework of a previously developed analytical coupled model, which described the mutual interaction across the sea surface of atmospheric and oceanic Rossby waves. A numerical model with the same physics is developed that permits the consideration of nontrivial background conditions. It is shown that the atmospheric modes that are least damped, and thus the patterns most easily energized by stochastic forcing, are neutral vectors.

1. Introduction

Low-frequency variability of the atmosphere in the midlatitudes, generated primarily by internal atmospheric dynamics, is dominated by a small number of characteristic patterns, of which the North Atlantic Oscillation (NAO) and the Pacific–North America (PNA) pattern are the most prominent (see, e.g., Wallace and Gutzler 1981; Barnston and Livezey 1987; Kushnir 1994). The underlying ocean is driven by these stochastic-in-time but coherent-in-space patterns of air–sea flux variability (see Cayan 1992). The ocean integrates over the (almost) white temporal ''noise'' producing a ''red'' power spectrum in oceanic variables (see, e.g., Frankignoul and Hasselmann 1977; Deser and Blackmon 1993; Sutton and Allen 1997; Czaja and Marshall 2001). If midlatitude SSTs can feed back on the modes of variability themselves, then coupled interactions can occur, thus reddening atmospheric spectra, too. Observations suggest that SST does have a small but discernible impact on, for example, the NAO (Czaja and Frankignoul 1999; Czaja and Marshall 2001), in agreement with the modeling studies of Rodwell et al. (1999), Mehta et al. (1999), and Watanabe and Kimoto (2000).

On seasonal to interannual timescales, thermodynamic aspects of the coupled system can be rather well described by stochastic climate models appropriately modified to allow for (i) feedback between SST and air temperature, as in Barsugli and Battisti (1998) or Bretherton and Battisti (2000); and (ii) reduced damping timescales of air–sea interaction resulting from the reemergence process[1] (e.g., Watanabe and Kimoto 2000). Several authors have developed simplified coupled models that, in addition to thermodynamics, also include atmosphere and/or ocean dynamics (Frankignoul et al. 1997; Jin 1997; Weng and Neelin 1998; Neelin and Weng 1999; Goodman and Marshall 1999; Cessi 2000; Gallego and Cessi 2000; Marshall et al. 2001; Ferreira et al. 2001).

The research described here attempts to identify what characterizes those dynamical modes of the atmosphere that couple most strongly with the underlying ocean. We find that ''neutral vectors''—the right singular vectors of the linearized atmospheric model's tendency matrix with the smallest eigenvalues (see Marshall and Molteni 1993; Navarra 1993)—act as pattern-specific amplifiers of ocean SST anomalies and dominate the coupled behavior. We believe that this is a rather general result that pertains not just to the simple model studies here, but to more complex models and perhaps also to the real coupled system.

We begin with a review of the mathematical devel-

* Current affiliation: Department of Geophysical Sciences, University of Chicago, Chicago, Illinois.

Corresponding author address: Dr. Jason C. Goodman, Department of Geophysical Sciences, University of Chicago, 5734 S. Ellis Ave., Chicago, IL 60640.
E-mail: goodmanj@uchicago.edu

[1] Thick winter ocean mixed layer temperature anomalies are covered in the summertime by a thin seasonal mixed layer. The following fall, these anomalies are exposed as the summer mixed layer erodes. Thus, winter SST anomalies seem to disappear in summer, and ''reemerge'' the following winter.

opment of neutral vectors and the ''optimal forcing patterns'' that excite them (section 2). This section recasts the work of Marshall and Molteni (1993) and Navarra (1993) in the light of coupled atmosphere–ocean interaction. In section 3, we illustrate the connection between neutral vectors and coupled modes using a numerical formulation of the coupled model considered (in analytical form) by Goodman and Marshall (1999, hereafter GM99). A substantial review of the dynamics of the GM99 model may be found in the appendix, along with our procedure for discretizing and solving the numerical model. This numerical model enables us to consider coupled dynamics in more complicated geometries and background states than the analytical GM99 model; we discuss the effect of these elaborations in section 3a. In section 3b, we analyze the behavior of the coupled model using singular vectors and find that the atmosphere's first neutral vector is the atmospheric component of the least-damped coupled mode; as a result, it dominates the stochastically forced system. These ideas suggest ways to use neutral vectors to investigate interannual atmosphere–ocean coupling in the observations and in more complex models, as described in section 4.

2. Neutral vectors and coupled modes

We begin by presenting the concepts underlying neutral vectors. The mathematical formalism presented here is a review of that found in Marshall and Molteni (1993) and Navarra (1993); our contribution here is the demonstration that these patterns are important in understanding atmosphere–ocean coupled modes.

a. Neutral vectors

Marshall and Molteni (hereafter MM) were interested in atmospheric wave patterns that tended to persist in a given state for long periods of time. They attempted to compute patterns of maximum persistence by beginning with a forced three-layer quasigeostrophic potential vorticity (QGPV) model, which we schematize as

$$\frac{\partial}{\partial t}\mathbf{q} = \mathcal{M}(\boldsymbol{\Psi}) + \mathbf{f},$$

where $\boldsymbol{\Psi}$ is a vector representing the model streamfunction, $\mathbf{q}$ is the model potential vorticity, $\mathcal{M}$ is a nonlinear tendency operator, and $\mathbf{f}$ is a potential vorticity source term. The model can be linearized by expressing $\mathbf{q}$ and $\boldsymbol{\Psi}$ as the sum of a given time-mean basic state plus a perturbation. The first-order perturbation equation can be written as

$$\frac{\partial}{\partial t}\mathbf{q} = \mathbf{M}\boldsymbol{\Psi} + \mathbf{f}, \tag{1}$$

where $\mathbf{q}$ and $\boldsymbol{\Psi}$ now represent perturbations about a specified basic state, and $\mathbf{M}$ is a perturbation tendency matrix. Marshall and Molteni were interested in the free, unforced perturbations that displayed the smallest time tendency. Free, unforced waves obey

$$\frac{\partial}{\partial t}\mathbf{q} = \mathbf{M}\boldsymbol{\Psi}. \tag{2}$$

To find the modes with the smallest time tendency, MM attempted to minimize this expression:[2]

$$\lambda^2 = \frac{\left\langle \frac{\partial}{\partial t}\mathbf{q}, \frac{\partial}{\partial t}\mathbf{q} \right\rangle}{\langle \boldsymbol{\Psi}, \boldsymbol{\Psi} \rangle}, \tag{3}$$

where the angle brackets $\langle \mathbf{a}, \mathbf{b} \rangle$ represent the inner product of $\mathbf{a}$ and $\mathbf{b}$. This expression minimizes the size of the mode's tendency, normalized by the magnitude of the mode itself. Inserting (2) into (3), we seek to minimize

$$\lambda^2 = \frac{\langle \mathbf{M}\boldsymbol{\Psi}, \mathbf{M}\boldsymbol{\Psi} \rangle}{\langle \boldsymbol{\Psi}, \boldsymbol{\Psi} \rangle} = \frac{\langle \mathbf{M}^\dagger\mathbf{M}\boldsymbol{\Psi}, \boldsymbol{\Psi} \rangle}{\langle \boldsymbol{\Psi}, \boldsymbol{\Psi} \rangle},$$

where $\mathbf{M}^\dagger$ is the adjoint of $\mathbf{M}$. The $\boldsymbol{\Psi}$ that minimize λ will be the eigenvectors $\boldsymbol{\Psi}_n$ of $\mathbf{M}^\dagger\mathbf{M}$ with minimum eigenvalue λ_n^2:

$$\lambda^2 = \frac{\langle \mathbf{M}^\dagger\mathbf{M}\boldsymbol{\Psi}_n, \boldsymbol{\Psi}_n \rangle}{\langle \boldsymbol{\Psi}_n, \boldsymbol{\Psi}_n \rangle} = \frac{\langle \lambda_n^2\boldsymbol{\Psi}_n, \boldsymbol{\Psi}_n \rangle}{\langle \boldsymbol{\Psi}_n, \boldsymbol{\Psi}_n \rangle}.$$

Marshall and Molteni call these smallest eigenvectors of $\mathbf{M}^\dagger\mathbf{M}$ the neutral vectors of the atmospheric model. They are the right singular vectors of $\mathbf{M}$ with the smallest singular values. At least one of the neutral vectors closely resembles a leading empirical orthogonal function (EOF) of the observed wintertime streamfunction fields (i.e., the NAO). We demonstrate and discuss the connection between EOFs and neutral vectors in a companion paper (Goodman and Marshall 2002). Neutral vectors are important because they identify the most prominent patterns of variability in the system from a *dynamical* framework. EOFs identify the most prevalent patterns in the data, but do not explain why those patterns appear. That neutral vectors have a close connection to EOFs is perhaps not surprising: the neutral vectors are, by design, the most stable and persistent wave patterns, so it makes sense that these patterns should be prevalent in observations. In fact, one can demonstrate (Goodman and Marshall 2002; Navarra 1993) that subject to certain restrictions, a mathematical identity exists between neutral vectors and the EOFs of a stochastically forced linearized model.

What are the dynamics of a neutral singular vectors? The matrix $\mathbf{M}$ describes Rossby wave propagation,

[2] Actually, MM wrote their equations as streamfunction tendencies, and minimized $\langle (\partial/\partial t)\boldsymbol{\Psi}, (\partial/\partial t)\boldsymbol{\Psi} \rangle / \langle \boldsymbol{\Psi}, \boldsymbol{\Psi} \rangle$. This has the advantage of allowing λ to be interpreted as an inverse timescale, but since modes with small streamfunction tendency must also have small PV tendency, the difference should be otherwise unimportant. The technique used here is computationally simpler and faster, and will make further developments more lucid.

downstream advection, and dissipation terms of the QGPV equation. For $\mathbf{M\Psi}$ to be small, dissipation must be weak (implying large-scale patterns), and there must be a near balance between the propagative and advective terms. Thus we can expect that neutral vectors will be ''resonant'' structures that can readily be excited.

Singular vectors are often applied to investigate the role of nonnormal growth to the production and maintenance of transient perturbations to the atmosphere, beginning with the study of Farrell (1982). A related problem considers the problem of optimal excitation patterns (see Farrell 1989; Molteni and Palmer 1993). The linear version of the principal interaction pattern/principal oscillation pattern (PIP/POP) techniques introduced by Hasselmann (1988) also use singular vectors to find patterns that best describe a system's tendency. The technique has also been used to find optimal amplification patterns in classic, nonrotating fluid dynamics (Andersson et al. 1999; Luchini 2000). However, in all the aforementioned applications the focus is on the singular vectors with the *largest* singular values—the most rapidly evolving and changing modes. Here our emphasis is on the physical relevance of the singular vectors with the *smallest* singular values.

b. Relevance of neutral vectors to coupled interaction

While MM were interested in the long-term stability of atmospheric wave patterns, we are interested in atmospheric patterns that are involved in coupled air–sea interaction. In particular, we wish to consider the possibility of a mutually coupled interaction, in which ocean SST anomalies force the atmosphere, which then feeds back on the ocean through wind stress, generating variability on interannual timescales. This type of interaction has been explored in simple models by GM99, Marshall et al. (2001), Gallego and Cessi (2000), Neelin and Weng (1999), and many others. We believe that neutral vectors are prime candidates for involvement in this class of interaction. Our reasoning is simple: if coupled modes are to occur, the atmosphere must respond strongly to the relatively small variations in atmospheric forcing generated by sea surface temperature anomalies. As we will now demonstrate, neutral vectors are the atmospheric modes that respond most strongly to PV forcing anomalies in a linearized model.

We return to the model in (1), but now we look at the forced, stationary response to an applied PV forcing $\mathbf{f}$:

$$0 = \mathbf{M\Psi} + \mathbf{f}.$$

What pair of forcing and response will have the largest response per unit forcing? We want to find the $\mathbf{\Psi}$ and $\mathbf{f}$ that will maximize

$$\lambda^{-2} = \frac{\langle \mathbf{\Psi}, \mathbf{\Psi} \rangle}{\langle \mathbf{f}, \mathbf{f} \rangle}.$$

Since $\mathbf{f} = -\mathbf{M\Psi}$, this is equivalent to *minimizing*

$$\lambda^{2} = \frac{\langle \mathbf{M\Psi}, \mathbf{M\Psi} \rangle}{\langle \mathbf{\Psi}, \mathbf{\Psi} \rangle}.$$

This is exactly the condition required for the neutral vectors. Thus, the neutral vectors are not only the most stationary modes in the unforced time-evolving model, they are also the forced, stationary modes that exhibit the largest response to external forcing.

Interestingly, this means we can not only find the neutral vectors, $\mathbf{\Psi}_n$, but also the optimal forcing patterns $\mathbf{f}_n$ that maximally excite them, by solving $\mathbf{M\Psi}_n + \mathbf{f}_n = 0$. The $\mathbf{\Psi}_n$ are the right singular vectors of $\mathbf{M}$; the $\mathbf{f}_n$ are the left singular vectors.

3. Neutral vectors and coupled modes in a simple coupled model

We now consider neutral modes in the context of a particular model of coupled interaction: that of GM99. A summary of this model maybe be found in the appendix. In brief, the model describes the linear interaction of traveling oceanic Rossby waves with forced stationary atmospheric planetary waves. The ocean is driven by wind stress and heat fluxes, while the atmosphere responds to thermal forcing from SST anomalies. The model produces a spontaneously growing coupled wave of subdecadal period and basin-filling horizontal wavelength. The positive feedback that produces this self-amplifying coupled mode is discussed in the appendix and at length in GM99.

As discussed in GM99, the coupled mode's atmospheric behavior is close to that of an atmospheric ''free mode'' in which there is an approximate balance between westward Rossby wave propagation and eastward PV advection by the mean atmospheric flow. This only occurs at a narrow range of wavelengths, so the coupled growth mechanism is highly scale selective.

Note that the balance exhibited by the atmospheric part of the coupled mode is exactly the balance satisfied by the neutral vectors. The $\mathbf{M}$ operator in (1) in large part describes the advection of PV anomalies by the mean flow and the advection of mean vorticity by the anomalous flow. The $\mathbf{\Psi}$ is a neutral vector when it causes cancellation of these terms, resulting in a small $\mathbf{M\Psi}$. Thus, only a small forcing is necessary to excite a large atmospheric response for this mode.

Of course, a large atmospheric response is only part of the story. In order to produce a mutually coupled interaction, SST anomalies must be actually able to produce a forcing that resembles the optimal forcing patterns. Moreover, the atmospheric response must drive the ocean in such a way as to enhance the original SST anomalies. The large atmospheric response to forcing exhibited by neutral vectors is a necessary but not sufficient condition for a coupled mode.

We will now demonstrate that the atmospheric component of the GM99 coupled model has neutral vector structure. This is not very remarkable (and has already

been described) for the extremely simplified case of uniform basic-state winds, as used in the GM99 model; however, we will also demonstrate a connection between neutral vectors and a coupled mode in the more realistic case of nonuniform basic-state winds. We will also demonstrate that when this model is excited by stochastic forcing, the atmospheric response is dominated by the coupled mode/neutral vector behavior. To enable this comparison, we have formulated the GM99 dynamics as a numerical model, discussed in the appendix.

a. Coupled dynamics with coastlines and varicose background flow

Before computing neutral vectors and comparing them with the coupled modes, it is important to note that the more realistic geometry enabled by the numerical coupled model causes some differences in behavior from the simple GM99 scheme. These extensions beyond GM99 must be understood in order to proceed, and are interesting in their own right.

The new features of the numerical model are the addition of coastlines to the ocean domain and the use of a nonuniform, varicose background flow in the atmosphere. We will consider the effects of these changes one at a time.

1) OCEAN BASIN

GM99's ocean and atmosphere had no boundaries. Here, we restrict the ocean domain to a basin 6000 km wide. The atmosphere lies within a 25 000-km zonally reentrant channel. ''SST'' anomalies over land are defined to be zero. Basic-state winds in the model's two atmospheric levels are 14 and 5 m s^{-1}. Other parameters are as specified in GM99.

We compute the eigenvalues of the model tendency operator for this single-basin model. Figure 1 shows the eigenvalues with the most positive real part. The growth rate of each eigenvector is given by its position on the x axis of the top panel; its frequency is given by its position on the y axis. Each complex-conjugate pair of eigenvalues corresponds to a pair of eigenvectors that are identical but for a 90° phase shift; phase propagation is always westward. Below the eigenspectrum, we display the eigenvector pattern corresponding to the rightmost eigenvalue pair. While the original GM99 model contained coupled growing modes (which would appear to the right of the origin in this figure), we see that when coastlines are added, all modes are damped. However, the structure of the rightmost, ''least-damped'' mode is quite similar to the coupled mode predicted by GM99. It displays equivalent barotropic wavenumber-3 structure in the atmosphere with matching wavelengths in the ocean, and high pressure over warm water—precisely the arrangement that grows most quickly in the analytical model. The wavelength of the mode seen in Fig. 1 matches the wavelength of maximum growth of the GM99 model.

The process that causes damping is easy to understand. SST anomalies in the GM99 model are dynamically connected to propagating oceanic baroclinic Rossby waves, and thus propagate westward. These Rossby waves are dissipated by interaction with the western boundary. A warm SST patch at the western side of the basin will excite the wavenumber-3 pattern characteristic of the atmosphere's equilibrated mode. This pattern will provide a wind stress forcing at the eastern side of the basin that creates a cool ''child'' SST anomaly to the west of the ''parent.'' For a growing mode to occur, the parent must bring the amplitude of the child up to its own amplitude before the parent is destroyed at the western boundary. This condition cannot be met with the choice of so narrow a basin (we have found that the critical basin width for these parameters is about 15 000 km), and so each parent produces a child weaker than itself, and the mode gradually dies away.

There are now no growing modes in this system; it only supports damped modes. However, if this system is excited with white stochastic forcing (as from atmospheric synoptic eddies), the least-damped mode should retain the most energy, and be the most prominent. Thus the feedback mechanism described in GM99 remains important in understanding the behavior of the present system. We will test this claim in section 3a(3).

The NAO and other observed patterns of interannual variability do not exhibit the rapid growth and puretone oscillations observed in GM99; instead, the NAO's time series spectrum (Hurrell and van Loon 1997) is predominantly reddish, with some apparent enhancement of power at interannual frequencies. In GM99, we noted the unrealistically rapid growth, and speculated that the unmodeled damping processes would counteract it. Such damping processes are readily observed in the present model.

2) VARICOSE ATMOSPHERIC BACKGROUND FLOW

We now attempt to study the effect of a more realistic atmospheric background flow on the model physics and proceed with a schematic formulation for the atmospheric stationary wave pattern. The midlatitude atmospheric flow at intermediate height exhibits a jet that constricts over the western shores of the Atlantic and Pacific, and is spread out over the eastern shores of the basins. We schematize this pattern by specifying a basic-state wind field that looks like Fig. 2. The zonally or meridionally averaged wind speed is constant and identical to the values used in the previous experiment.

For this experiment, we illustrate the behavior of the coupled model by integrating it forward in time. The model is initialized with random SST and ocean streamfunction anomalies of arbitrary amplitude, and stepped forward using a simple Euler forward scheme, with a 30-day time step. Figure 3 shows the evolution of the

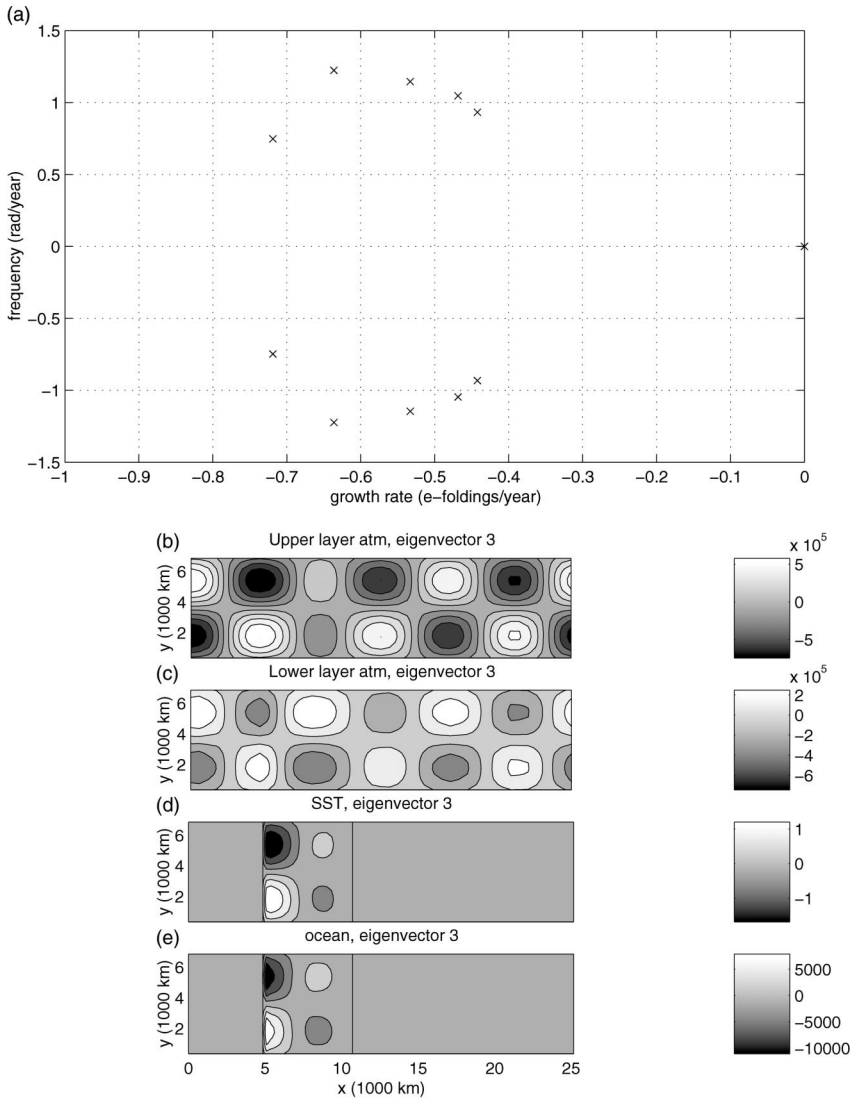

FIG. 1. GM99 model with parallel channel atmospheric background flow, ocean confined to 6000-km-wide basin. (a) Eigenvalues of the coupled model's tendency matrix. (b)–(e) Real part of eigenvector associated with the eigenvalue with largest real part.

model with an ocean basin identical to that in section 3a(1), and with basic-state winds as shown in Fig. 2. The upper four panels of Fig. 3 show a snapshot of anomalies of upper- and lower-layer atmospheric streamfunction, SST, and ocean streamfunction. The Hovmoeller diagrams in the lower left show the evolution of SST anomalies and of lower-level atmospheric perturbations. Perturbations decay to zero, as before, due to the destruction of oceanic anomalies at the western boundary. Oscillation and damping rates are similar the parallel-flow model, and the atmospheric wave pattern again generally shows equivalent barotropic wavenumber-3 behavior, although some additional elements are present. The atmospheric wave no longer propagates westward in phase with SST anomalies; instead, it remains more or less fixed at a particular longitude, and fluctuates in sign. The varicose background flow locks the atmospheric response to a particular longitude, which is more reminiscent of observed patterns of low-frequency variability.

The SST pattern of this system is more complex than the simple propagating wave pattern of previous experiments, but generally shows westward-propagating patches of warm and cool water.

3) RESPONSE TO STOCHASTIC FORCING

In section 3a(1), we noted that when confined to a basin, the coupled mode no longer grew, but remained the least-damped mode. We argued that the least-damped mode would be most susceptible to excitation by stochastic forcing. In this section, we test this claim.

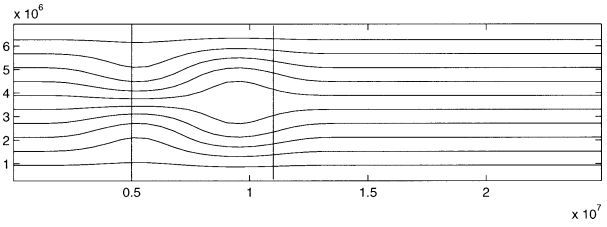

FIG. 2. Basic-state streamfunction pattern used in the varicose background flow experiment. The basic-state streamfunction is given by the relation $\psi = U_0 y + 0.1U_O(L_y/2)F(x, y)$, where $F(x, y) = \sin(2\pi y/L_y)\sin^2(\pi y/L_y)\sin[4\pi(x - x_0)/L_x]\sin^2[2\pi(x - x_0)/L_x]$ when $x > x_0$ and $x < (L_x/2 + x_0)$, and $F(x, y) = 0$ elsewhere. Here U_O is the wind velocity in either level from the uniform-flow experiment, x_0 is 10^6 m, and L_x and L_y are the zonal and meridional extents of the channel.

We consider the case of a varicose background atmospheric flow over an ocean basin, as in section 3a(2), and carry out a long forward integration of the model, as in Fig. 3. But now, at each time step, after computing the atmospheric response to SST (ψ_1, ψ_2), we randomly generate an additional stochastic streamfunction component (ψ_{1s}, ψ_{2s}), add it to the response, and use the result to force the SST and dynamic ocean parts of the coupled model [Eq. (A3) and Eq. (A4) in appendix, respectively].

The stochastic components of the atmospheric fields are chosen to very roughly mimic the structure and amplitude of transient eddies in the atmosphere. At each model time step ($\Delta t = 1$ month) we generate a Gaussian random streamfunction field, spectrally truncated to zonal wavenumber 8 and meridional wavenumber 3. Thus the smallest wavelengths are around 3000 km. We multiply this by $\sin(\pi y/L_y)^{0.7}$ to bring the eddy amplitude to zero at the northern and southern walls, thus avoiding boundary condition problems. We multiply this field by an amplitude factor of 180 geopotential meters (gpm) in the upper layer and 120 gpm in the lower layer, to create an equivalent barotropic streamfunction pattern. These fields drive the ocean through the air–sea heat flux term and wind stress curl.

In Fig. 4, we show snapshots of the model state, and its evolution through time. The atmospheric components plotted here are only the deterministic responses to SST; the additional random component is not shown in these figures. As we would expect, the stochastic model's evolution is much less orderly. However, the patterns of atmospheric response show the wavenumber-3 by wavenumber-1 mode previously identified as a coupled mode, though the resemblance is not always as strong as in this snapshot. SST anomalies show westward propagation, and both atmospheric and oceanic variables show strong interannual variability. The amplitude of SST anomalies is of the order of a degree or so, with atmospheric responses of a few tens of geopotential meters; these amplitudes are similar to, but somewhat larger than, those observed on interannual timescales in the Atlantic (see Czaja and Marshall 2001). These amplitudes are determined entirely by the strength of stochastic forcing, but we chose a stochastic amplitude based on observed wintertime synoptic activity, and did not tune it to improve the resemblance of the coupled response to observations.

To more clearly isolate the dominant patterns of variability, we perform an EOF analysis on the upper-atmospheric streamfunction field—the EOFs are shown in Fig. 5. The first EOF explains 56% of the *nonstochastic part* of the atmospheric variability; the second EOF explains 35%, and the third EOF, 5%. The first EOF shows a predominantly zonally symmetric pattern, with no clear pattern to its variability and only a weak covarying oceanic pattern (not shown). This mode reacts strongly to SST anomalies, but is unable to excite a mutually coupled interaction. We will revisit this pattern in section 2a. The second and third EOFs are much more interesting. They show wavenumber-3 structure; the patterns are essentially identical to the atmospheric component of the least-damped coupled mode depicted in Fig. 3. [The shape of the atmospheric pattern in section 3a(2) varies periodically; it tends to oscillate between a state resembling EOF 2 and a state resembling EOF 3.] A 5-yr cycle is apparent in the amplitude timeseries of EOF 2, the timescale set by the propation speed of SST anomalies in the ocean controlled here by Rossby wave dynamics; a similar frequency is present (though less obvious) in the time series of EOF 3. The amplitude of EOF 2 is about 10% of the total atmospheric amplitude, including both stochastic and deterministic contributions. As anticipated, the least-damped coupled mode previously discussed does, in fact, explain a large amount of the stochastic model's variability.

We now discuss how the coupled interaction can be interpreted and understood in terms of neutral vectors.

b. Interpretation of coupled interaction in terms of neutral vectors

To compute the neutral vectors of the atmospheric component of the model, in both constant zonal flow [section 3a(1)] and varicose flow [section 3a(2)] arrangements, we use an Arnoldi (Lehoucq et al. 1998) technique to yield the smallest five singular vectors of the model atmosphere's tendency matrix **M**. To perform this computation, we must specify a particular inner product in (3): here, we define $\langle \mathbf{a}, \mathbf{b} \rangle$ as the sum over all model grid points of the products of **a** and **b** evaluated at each grid point. Other, differently weighted inner products are possible, but our results are not sensitive to this choice.

The first five neutral vectors for the constant zonal flow model (not shown) only vary meridionally, and have no zonal structure. As such, they are unaffected by zonal advection or Rossby wave propagation: they are ''neutral'' in a rather trivial way. The first neutral vectors with zonal structure are the sixth and seventh ones; they display wavenumber-3 structure zonally, and wavenumber-1 zonally, and are 90° out of phase with

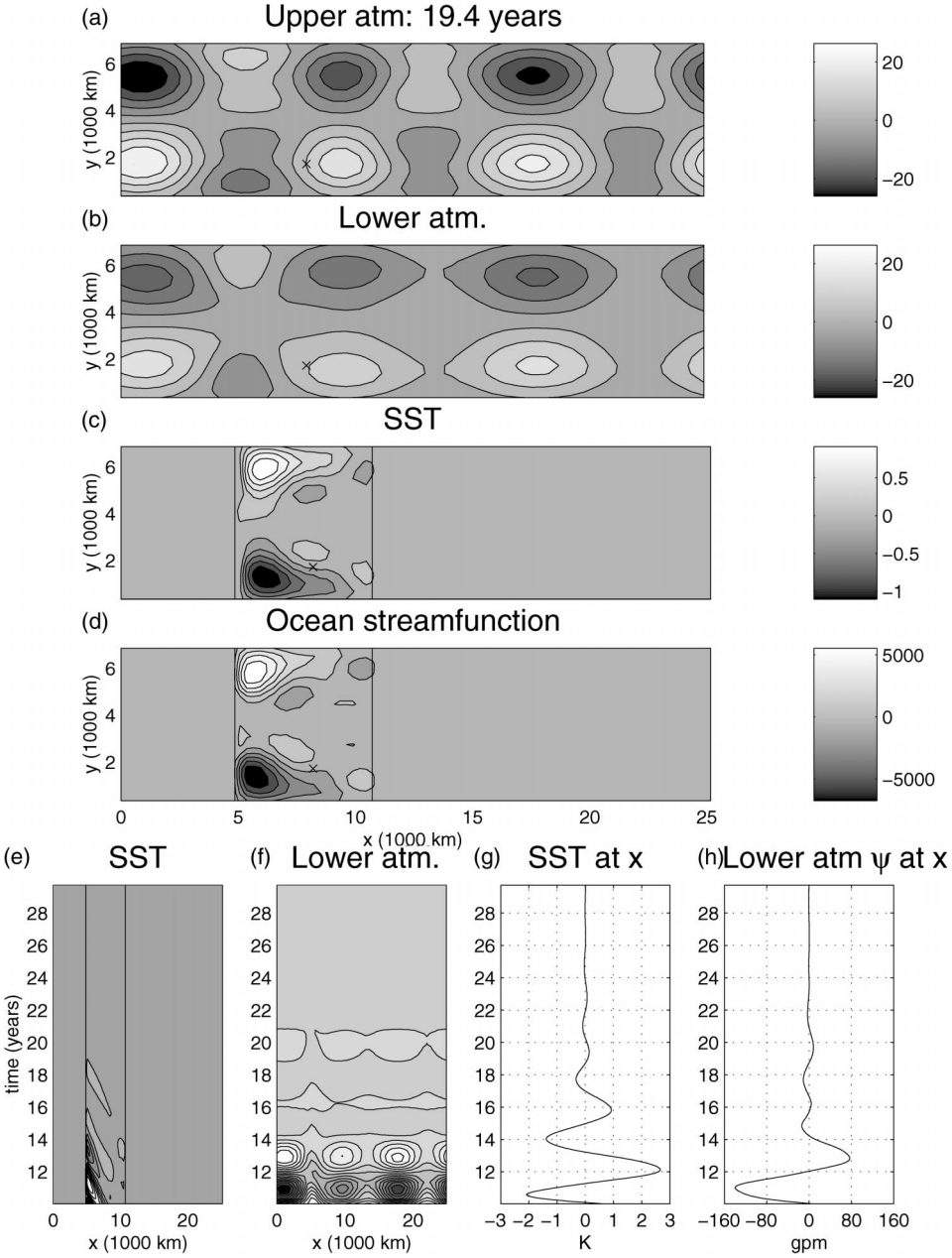

FIG. 3. Snapshots and evolution of the numerical model, run with a basin ocean and varicose background flow. The model was initialized with random values in SST and ocean streamfunction. (a), (b) The upper- and lower-atmospheric streamfunction anomalies (ψ_1, ψ_2), expressed as geopotential height (in m) of pressure surfaces. (c), (d) The SST anomalies, in K, and ocean streamfunction anomalies, in $m^2\ s^{-1}$. (e), (f) Time–longitude sections of SST and ψ_2, taken at the latitude of the small "×" in the upper panels. (g), (h) A time series of SST and ψ_2, taken at the ×.

each other. Their structure matches that of the coupled mode found in section 3a(1).

In Fig. 6, we show the three leading neutral modes for the atmosphere with a varicose background flow discussed in section 3a(2). The first neutral vector is a zonal mode analogous to the modes with no zonal structure found above. The second and third neutral vectors display structures nearly identical to the structure of the coupled mode in section 3a(2). Neutral vectors 1, 2, and 3 are identical in pattern and order to the EOFs of the stochastically forced coupled model (see Fig. 5).

This provides a demonstration that the neutral vectors continue to determine the behavior of the atmospheric component of the coupled system, even when the atmosphere has a complicated background flow.

How are these neutral vectors excited in the coupled

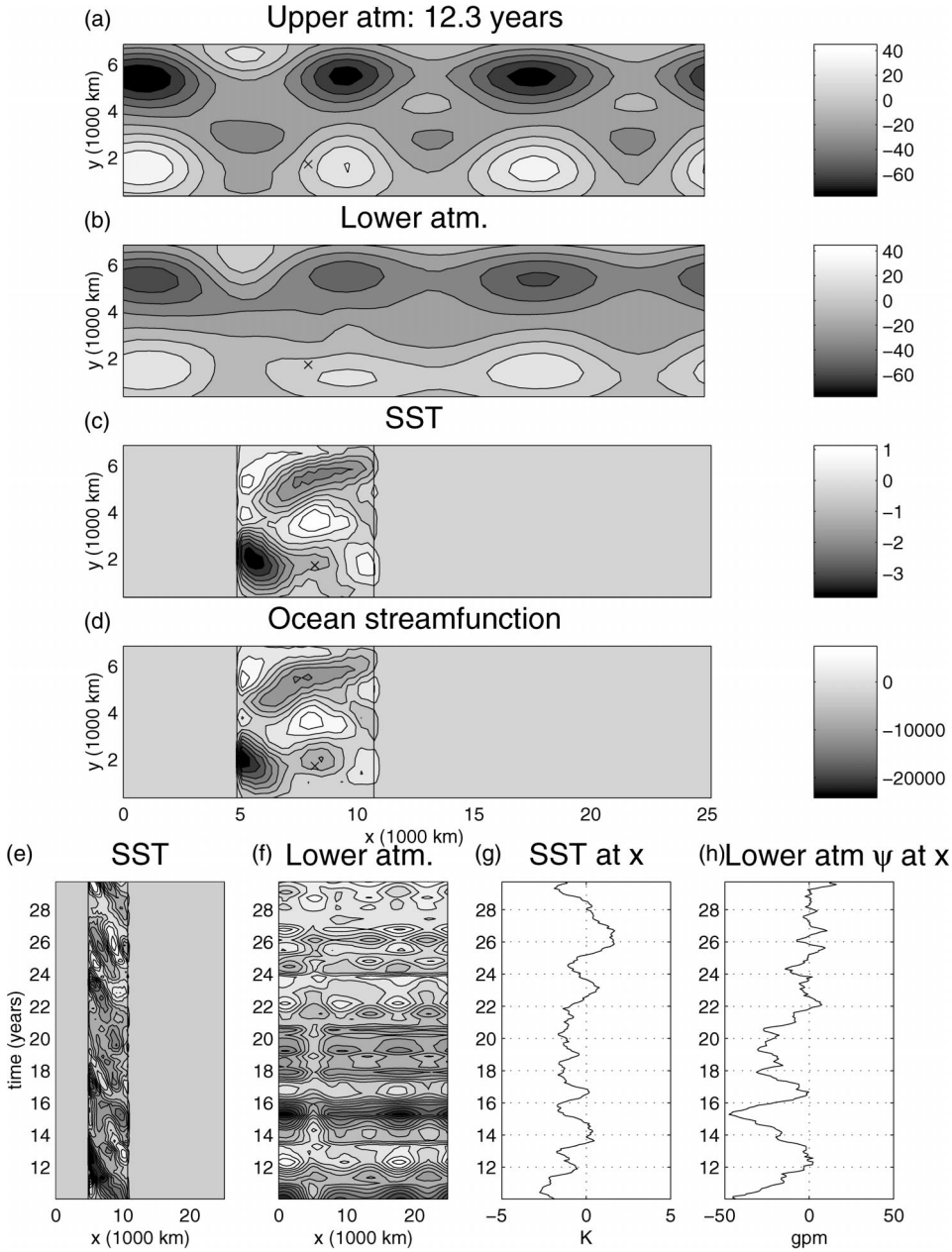

FIG. 4. Same as Fig. 3, but with stochastic forcing added. The rms amplitude of stochastic atmospheric perturbations is 180 gpm in upper layer, 120 gpm in lower layer. Only the deterministic part of the atmospheric perturbation is shown here. Atmospheric perturbations are expressed in gpm; units of SST are K, units of ocean streamfunction are $m^2\ s^{-1}$.

model? This model has a very simple atmospheric heating scheme: there is a linear connection between SST and baroclinic PV forcing as discussed in the appendix. Thus, when the coupled model's SST has a strong projection onto the baroclinic part of an optimal forcing pattern $\mathbf{f}_n$, we see a corresponding strong atmospheric response of the corresponding neutral vector.

Figure 7 more clearly displays the interaction between atmospheric neutral vectors and evolving SST anomalies in the GM99 model. At the top of the figure, we show the upper-level streamfunction of neutral vectors 2 and 3 for the varicose background flow model; these are the neutral vectors that resembled the coupled model's behavior. The upper time series shows the projection of the model's atmospheric state onto the first five neutral vectors. Since the model ocean has a western boundary, the model response is damped. We have thus multiplied the projection values by $e^{t/3}$ (where t is given in yr), to counteract the exponential decay and zoom in on the longer-term variations. We clearly see the oscillation

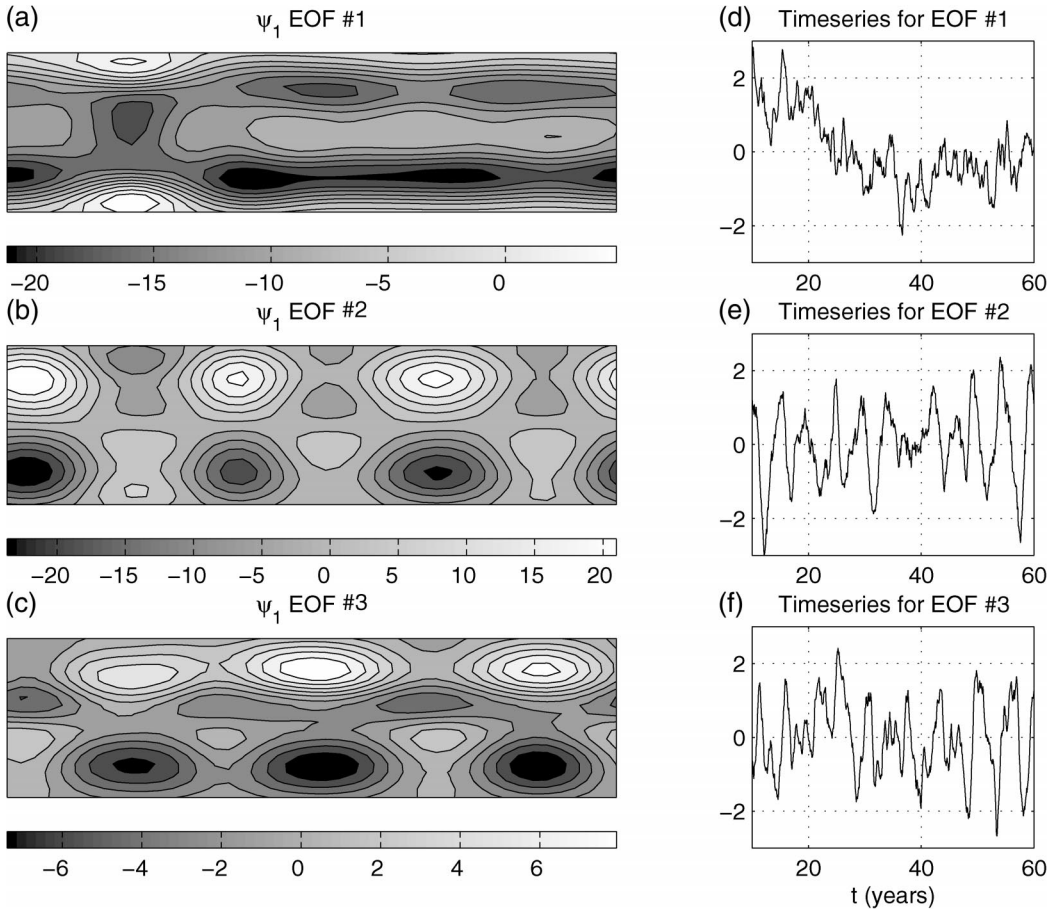

FIG. 5. EOFs of the upper-layer atmospheric streamfunction for the stochastically forced coupled model run depicted in Fig. 4. (a)–(c) EOF patterns; (d)–(f) corresponding amplitude time series. (a), (d) Pattern and time series for first EOF, which explains 56% of the deterministic variability. (b), (e) Second EOF, explaining 35% of the deterministic variability. (c), (f) Third EOF, explaining 5% of the deterministic variability.

of the model state between neutral vectors 2 and 3, as described in the previous section. The lower pair of contour plots show the baroclinic part of the optimal forcing pattern associated with these neutral vectors. The lower time series shows the projection of the thermal forcing anomalies generated by SST onto the first five optimal forcing patterns, rescaled as with the neutral vector time series. The match is identical, as a consequence of the linearity of the atmospheric response operator.

From Fig. 7, we can describe the behavior of the coupled mode. As the model's SST pattern evolves according to ocean dynamics, it projects alternately onto two different optimal forcing patterns. This projection excites a large atmospheric neutral vector response, which then provides a wind stress to further modify the SST.

Neutral vectors 2 and 3 are active in the coupled interaction. Patterns that are less neutral (modes 4 and up) respond only weakly to SST forcing, undergo a much weaker coupled interaction, and are more rapidly damped. As mentioned earlier, a strong atmospheric response to thermal forcing is a necessary, but not sufficient, condition for a mutually coupled mode: neutral vector 1 responds strongly to SST forcing, but does not feed back onto the model ocean in a way that leads to positive feedback.

One point of concern regarding this description is the robustness of the optimal forcing patterns. In Fig. 7, the optimal forcing patterns show complicated fine structure in some areas (particularly near $x = 5000$ km, $y = 3200$ km, in the ''pinched'' part of the background flow; there, we find an alternating positive/negative banded pattern at the grid-scale level). This may be due to the minimal eddy viscosity used in this model. If most of the SST forcing pattern's projection onto this pattern occurs in this fine-structure region, we should be concerned that the stability of the coupled mode is sensitive to small changes in the model domain. However, we find (figure not shown) that the bulk of the projection of SST onto the forcing pattern occurs in the broad ''wings'' to the north and south in forcing pattern 2, and to the northeast and southeast in pattern 3.

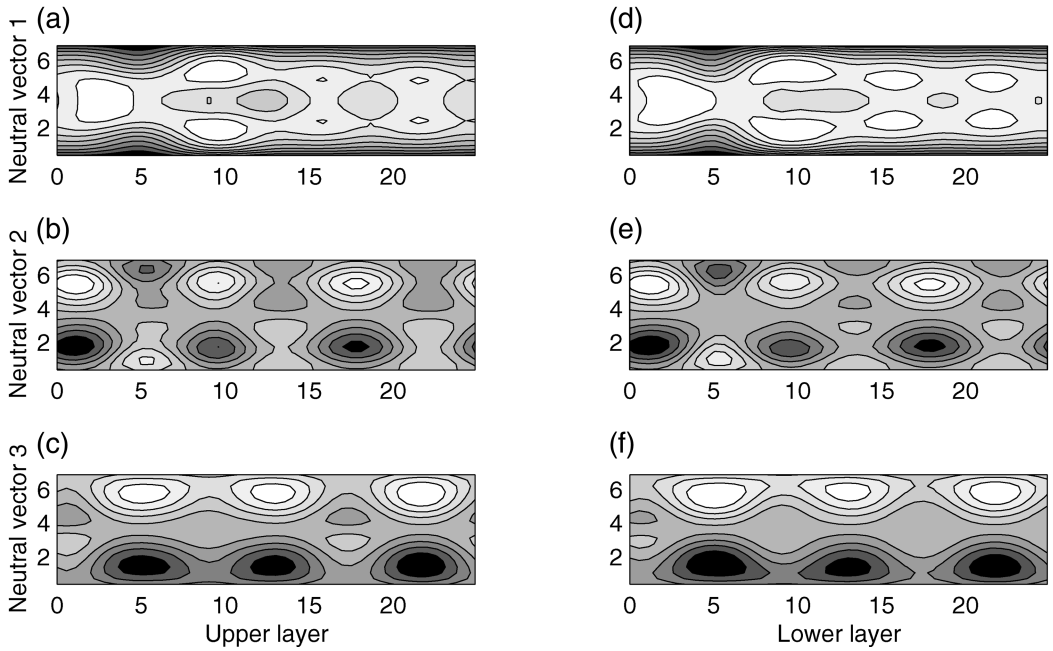

FIG. 6. Maps of the first three neutral vectors of the atmospheric model with a varicose background flow as pictured in Fig. 2. (a)–(c) Upper-level streamfunction. (d)–(f) Lower-level streamfunction.

4. Conclusions

Neutral vectors are the singular vectors of a linearized model's tendency matrix with smallest singular value. We have demonstrated mathematically that neutral vectors are also the patterns that respond most strongly when the model is externally forced. Moreover we have shown that neutral vector dynamics (an approximate balance between advection of the mean PV by a flow perturbation and advection of the perturbation's PV field by the mean flow) are responsible for the atmospheric part of the coupled growing mode found in Goodman and Marshall's (1999) simple atmosphere–ocean coupled model.

We proceeded to illustrate the generality of this connection by building a numerical model that obeys the coupled physics desribed in GM99, but that allows for more complex geometry and nonuniform basic-state flows. The added complexities change the system's behavior (a western boundary current damps the mode; varicose atmospheric background flow locks the atmospheric mode to particular longitudes), but the coupled mechanism described by GM99 remains important. The atmospheric patterns involved in the coupled interaction are still neutral vectors.

In our coupling mechanism, the optimal forcing pattern/neutral vector pair can be viewed as a mechanism that accepts a small SST thermal forcing from the ocean and returns a large atmospheric response, which may translate into a large feedback onto the ocean. However, this is only half the story: the ocean must be able to accept the forcing provided by the atmosphere and return (some nontrivial projection onto) the neutral vector's optimal forcing pattern in order for a mutually coupled interaction to occur. Optimal forcing pattern/neutral vector pairs may play a key role as pattern-selective amplifiers in a coupled atmosphere–ocean system.

The atmospheric model used in this study is linear and steady state. High-frequency variability and the nonlinear feedback of this variability onto the mean flow are not modeled explicitly. However, synoptic variability is crucial to the coupling mechanism. It stochastically forces the slowly varying coupled system; the coupled mode responds most strongly to this forcing, and becomes prominent. More complicated eddy–mean flow interactions lie outside the scope of this simple model. We discuss the feasibility of incorporating eddy–mean flow interaction into a neutral vector calculation in a companion paper (Goodman and Marshall 2002).

The ocean component of the numerical coupled model developed for this work could easily be extended to let us impose nonzero basic-state currents (a double-gyre flow, for example), but we have not considered this important case here. An imposed ocean current would advect SST and oceanic PV anomalies around the ocean basin. Even if the ocean currents dominate the Rossby wave propagation seen here, a coupled oscillation is still possible. As SST anomalies are transported around a gyre, they will excite neutral vector responses from the atmosphere. If the surface fluxes caused by any neutral vector act to enhance the original SST anomaly pattern, a growing coupled mode will still occur, with the mode's oscillation period now given by the gyral recirculation time, rather than the Rossby wave period.

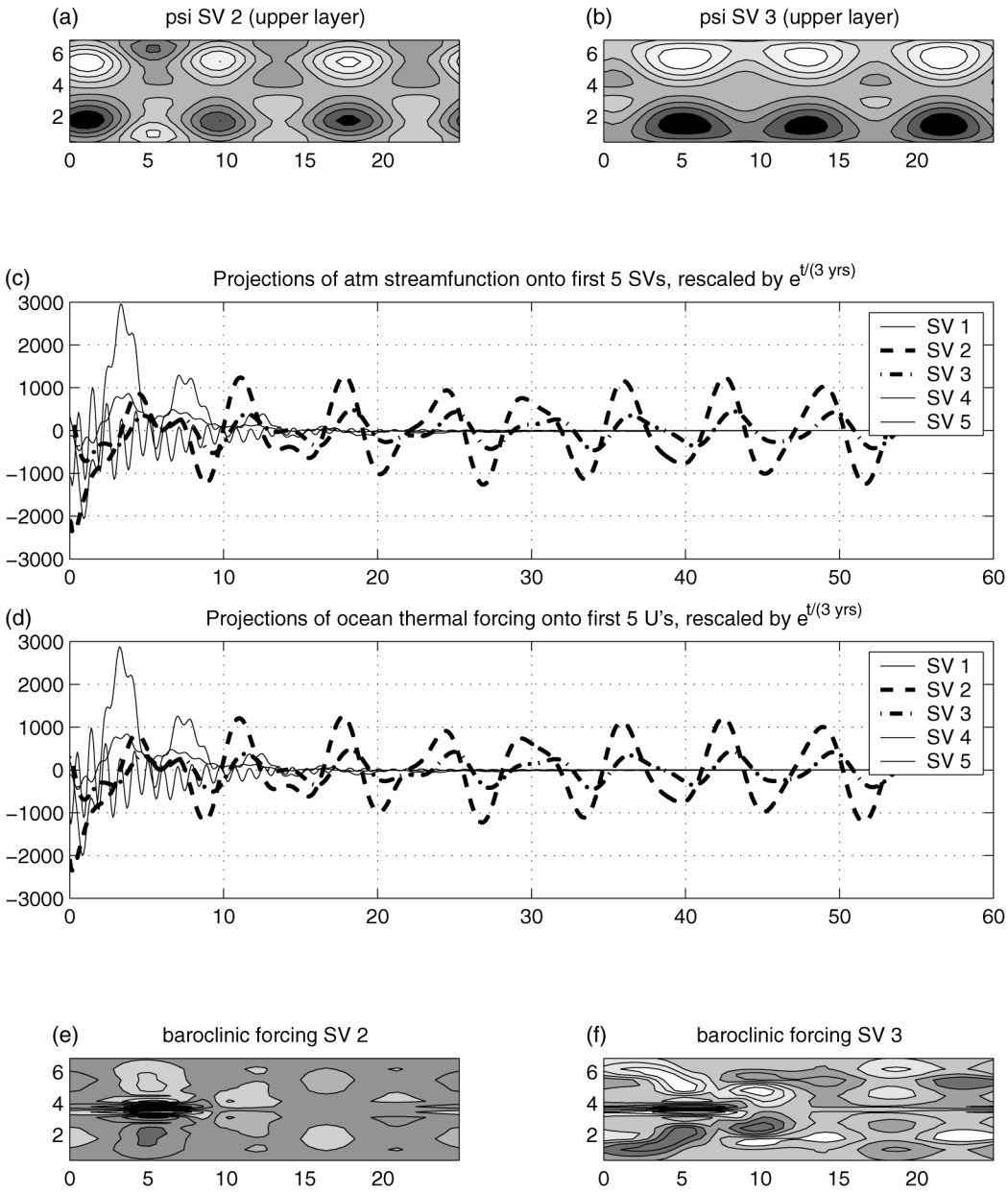

FIG. 7. Projections of neutral vectors and optimal forcing patterns onto a forward model run. (a), (b) Upper-layer streamfunction pattern for neutral vectors 2 and 3; respectively, of the atmospheric model with a varicose jet background flow. (c) The projection of the time evolution of the coupled model's atmosphere onto singular vectors 1–5. (d) the projection of SST-induced atmospheric thermal forcing onto the first five optimal forcing patterns. (e), (f) The baroclinic part of the PV forcing that excites neutral vectors 2 and 3 (''optimal forcing patterns''; see text).

Our model is extraordinarily crude, and so we should not expect the particular shapes and patterns of the coupled mode and the atmospheric neutral vectors to correspond in detail with observed patterns, although the broad correspondence is promising. However, the physical mechanism of coupling (excitation of neutral vectors by SST forcing) can be applied in much more realistic situations. Our results suggest that neutral vectors are likely to be important for atmosphere–ocean interaction in a very general sense.

In a companion paper (Goodman and Marshall 2002), we return to Marshall and Molteni's (1993) three-layer QG model, to look more closely at the connection between neutral vectors and EOFs, and to compute optimal forcing patterns associated with neutral vectors. If we can identify a forcing pattern that induces a particular mode of atmospheric variability, then it can be used to see whether the patterns of SST that covary with, for example, the NAO pattern, are those that are capable of exciting that pattern.

The identification of neutral vectors is not limited to simple QG models with trivial model physics. The tendency matrix **M** can be arbitrarily complex: it could even represent an entire atmospheric general circulation model, linearized about some suitable basic state. The $\mathbf{M}^{\dagger}$ matrix is then the adjoint of this model. It is thus possible to find the neutral vectors of an entire linearized GCM, along with the corresponding optimal forcing patterns. This is, as one might imagine, a computationally intensive task. However, the implementation could be made easier through the use of an automatic tangent linear/adjoint compiler (Marotzke et al. 1999), which can automatically generate adjoint model code from the forward source.

The neutral vector concept can be generalized to almost any model physics, and will be relevant to the investigation of atmosphere–ocean coupled modes whenever the atmosphere responds to SST forcing anomalies in an essentially linear way, and when a large atmospheric response will produce a large forcing of the ocean by the atmosphere.

Neutral vectors will respond strongly to any forcing source, regardless of its origin. Thus, they may shed some light on observations that the same observed patterns of variability (NAO, PNA, etc.) dominate atmospheric variability on both short (intramonthly) and long (interannual) timescales. It is possible that the long-term variability is simply the low-frequency tail of a high-frequency stochastic process, but it is also possible that these patterns represent atmospheric neutral vectors responding both to random high-frequency forcing by synoptic eddies and to coherent low-frequency forcing driven by SST.

Acknowledgments. This work was supported by the NOAA Office of Global Programs.

APPENDIX

The GM99 Coupled Model

a. Dynamical framework

In this section, we summarize the results of Goodman and Marshall (1999, hereafter GM99), which provides the foundation upon which our ideas are developed.

The GM99 model (Fig. A1) incorporates a 1½-layer quasigeostrophic ocean anomaly model in an unbounded domain. In this model, undulations of the layer interface lead to surface currents and propagating Rossby waves. A basic state at rest is prescribed. The QG ocean forces a simple mixed layer model, which incorporates storage, advection, air–sea transfer, and mixed layer entrainment processes. The sea surface temperature anomalies produced by this mixed layer model thermally excite a two-level quasigeostrophic atmospheric anomaly model, whose basic state has constant uniform zonal winds of differing magnitudes in the two layers. Basic-state winds are chosen to resemble wintertime conditions: the annual cycle is not resolved. The atmospheric pressure anomalies drive the QG ocean through surface wind stress, allowing mutual coupling of atmosphere and ocean.

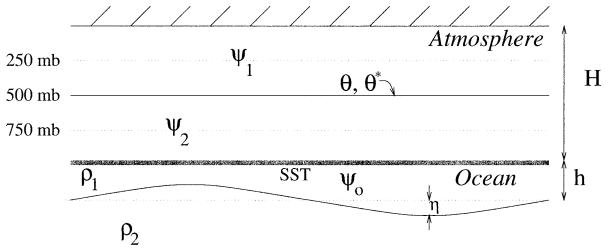

FIG. A1. Vertical structure of the coupled model defining the key variables of the GM99 model.

This physics is expressed in the following set of linear partial differential equations that represent first-order balances for linear perturbations about a basic state.

- Atmosphere (upper level):

$$J(\psi_1, Q_1) + J(\Psi_1, q_1) = \frac{\gamma_a}{L_a^2}\left[(\psi_1 - \psi_2) - \frac{\mathrm{SST}}{r_a}\right]. \quad \text{(A1)}$$

- Atmosphere (lower level):

$$J(\psi_2, Q_2) + J(\Psi_2, q_2) = -\frac{\gamma_a}{L_a^2}\left[(\psi_1 - \psi_2) - \frac{\mathrm{SST}}{r_a}\right]. \quad \text{(A2)}$$

- SST:

$$\frac{\partial}{\partial t}\mathrm{SST} = -\gamma_o[\mathrm{SST} - r_a(\psi_1 - \psi_2)] - J(\psi_o, \overline{\mathrm{SST}}) - \gamma_e(\mathrm{SST} - r_o\psi_o). \quad \text{(A3)}$$

- Dynamic ocean:

$$\frac{\partial}{\partial t}q_o + \beta\frac{\partial}{\partial x}\psi_o = \alpha\nabla^2\left(\frac{3}{2}\psi_2 - \frac{1}{2}\psi_1\right). \quad \text{(A4)}$$

In the above, Ψ_1 and Ψ_2 are the basic-state atmospheric streamfunctions; ψ_1, ψ_2, ψ_o are the streamfunction anomalies in the upper- and lower-atmospheric layers and in the ocean; $\theta_a = r_a(\psi_1 - \psi_2)$ is the atmospheric temperature; Q_1 and Q_2 are the basic-state atmospheric PV fields; and q_1, q_2, and q_o are the QG potential vorticity anomalies in the atmosphere and ocean. $\overline{\mathrm{SST}}$ and SST are the unperturbed and anomalous sea surface temperature; the term on the right-hand side of Eq. (A4) is the mechanical forcing of the ocean by the winds extrapolated down to the surface (α is a drag coefficient); terms on the right-hand sides of Eqs. (A1) and (A2) represent a baroclinic thermal forcing via relaxation of the atmospheric temperature anomaly θ_a to a value set

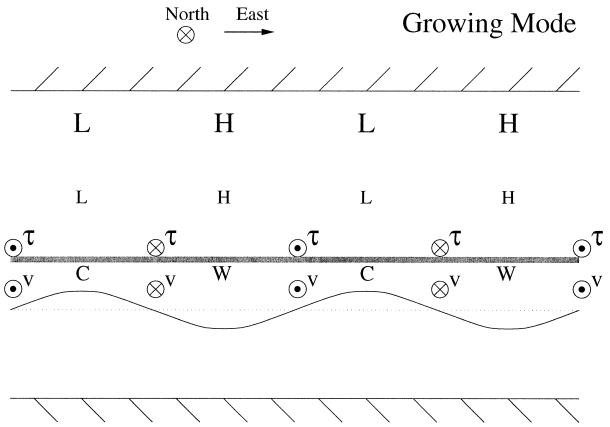

FIG. A2. Phase relationships between ocean and atmosphere for the fastest growing coupled mode found by GM99. The symbols H and L denote highs and lows of atmospheric pressure, with the amplitude of the pressure anomaly increasing with height. The symbols W and C denote warm and cold SST, and the undulating line indicates the depth of the thermocline. Note the high (low) pressure above warm (cold) water, and the phase match between wind stress and current.

by SST; and the forcing terms for SST represent air–sea heat flux, advection of the mean SST gradient, and entrainment, in that order. The parameters r_a and r_o are conversion constants for translating streamfunctions into temperatures via the thermal wind equation, in the atmosphere and ocean, respectively. All notations and definitions are identical to those in GM99.

In GM99, simplifications are made such that this set of equations is linear and has constant coefficients. Thus, they can be solved by inserting plane-wave solutions and solving for the dispersion relation. Within a narrow band of wavelengths, a coupled growing wave is possible. As discussed in GM99, this wave has a frequency of about 5–8 yr and an *e*-folding growth timescale of about 2 yr, given plausible (but rather uncertain) parameters.

Figure A2 illustrates the structure and physics of this growing mode. The mixed layer entrains fluid from the stratified ocean interior into itself. When the thermocline is bowed upward, this fluid will be anomalously cool; when the thermocline is bowed downward, it will be warm. This leads to a correlation between a deep thermocline and warm SST, and vice versa. Even in the absence of entrainment, this correlation still exists due to geostrophic advection in the mean SST gradient—see section 3b(1) of GM99 for details.

Suppose the thermocline is bowed upward, causing a cold SST anomaly. For particular zonal and meridional wavelengths, this will generate an equivalent-barotropic low pressure anomaly in the atmosphere, centered above the cool SST. This low pressure anomaly will induce a cyclonic wind stress curl to the ocean, causing upward Ekman pumping, raising the already shallow thermocline, and making SST even colder. This is a coupled positive feedback. While this feedback is occurring, the thermocline anomaly propagates westward as a Rossby wave.

The growth mechanism can only operate when the atmospheric response is characterized by equivalent barotropic highs (lows) over warm (cold) water. This occurs only in a rather narrow band of wavelengths for which downstream advection balances upstream Rossby wave propagation; that is, for winds, potential vorticity gradients, and scales that are close to that of a neutral state of the atmosphere (i.e., free stationary Rossby waves). For reasonable parameter choices, this scale-selective growth mechanism selects a wavelength close to that of the NAO pattern.

In order to allow solution by hand, the GM99 model is oversimplified in many ways. Among these are its constant zonal basic-state winds, the lack of a reentrant atmospheric geometry, the use of only two levels in the atmosphere, the lack of coastal boundaries in the ocean, and the absence of basic-state currents in the ocean. In the next section, we develop a model in which we can relax some of these simplifications.

b. Numerical model formulation

We begin with the same differential equations (A1)–(A4) as in GM99. In GM99, we assumed that Ψ_1, Ψ_2, Q_1, and Q_2 were linear functions of the meridional coordinate (i.e., the basic-state flows were constant and purely zonal) to make analytic solution tractable. Here we allow for the possibility that the ocean is of restricted east–west extent, and study the effect of nonuniform atmospheric flows. The important case of nonzero basic-state ocean currents will not be considered here.

For arbitrary basic states, the system of Eqs. (A1)–(A4) must be solved numerically. We do this by forming finite-difference forms of the equations above. To allow solution in a rectangular oceanic domain, we must add a Stommel (1948) frictional term to Eq. (A4), permitting a western boundary current to form. We must also be careful to write the finite-difference forms of the advection operators in (A1) and (A2) so that they conserve PV exactly. We also added a small amount of vorticity diffusion and dissipation of PV anomalies into the model atmosphere for numerical stability.

The model is discretized using a standard finite-difference scheme, with ψ- and q-points coincident, and using a centered difference scheme for first derivatives and a five-point stencil for the Laplacian operator. We specify a periodic channel geometry in the atmosphere whose zonal and meridional extents are 25 000 and 7200 km, respectively. The north and south boundary conditions in the atmosphere are designed to allow no PV flux through the walls. The meridional grid spacing is 360 km; the zonal grid spacing is 550 km in the atmosphere and 275 km in the ocean. Upon discretization, the SST and ocean streamfunction equations can be written in the form

$$\frac{\partial}{\partial t}\begin{bmatrix}\mathbf{SST}\\ \boldsymbol{\Psi}_o\end{bmatrix} = \mathbf{P}\begin{bmatrix}\boldsymbol{\Psi}_1\\ \boldsymbol{\Psi}_2\\ \mathbf{SST}\\ \boldsymbol{\Psi}_o\end{bmatrix}, \tag{A5}$$

where $\mathbf{SST}$, $\boldsymbol{\Psi}_o$, $\boldsymbol{\Psi}_1$, and $\boldsymbol{\Psi}_2$ are vectors containing the discretized elements of the SST, ocean streamfunction, and atmospheric upper- and lower-layer streamfunction anomaly fields. The matrix $\mathbf{P}$ is a sparse matrix representing the finite-differenced forms of the differential operators in (A4) and (A3). We must find $\boldsymbol{\Psi}_1$ and $\boldsymbol{\Psi}_2$ using the side constraints provided by (A1) and (A2):

$$\mathbf{M}\begin{bmatrix}\boldsymbol{\Psi}_1\\ \boldsymbol{\Psi}_2\end{bmatrix} = \frac{\gamma_a}{L_a^2 r_a}\begin{bmatrix}-\mathbf{SST}\\ \mathbf{SST}\end{bmatrix}, \tag{A6}$$

where $\mathbf{M}$ is a matrix incorporating discretized forms of the advection and dissipation operators acting on the atmospheric state vectors. It is identical to the $\mathbf{M}$ used in (1) and throughout section 2.

c. Time evolution and eigenspectrum

We can step the system forward in time by inverting (A6) to find $\boldsymbol{\Psi}_1$ and $\boldsymbol{\Psi}_2$ at each time step from $\mathbf{SST}$, then plugging those into (A5) to get the rate of change of $\mathbf{SST}$ and $\boldsymbol{\Psi}_o$, which can then be advanced to the next time step using a simple Euler forward scheme.

We can also solve for the eigenvectors of the system's tendency matrix; this allows us to compute frequencies and growth/decay rates for the coupled mode, as done in GM99 for the simpler case of plane-parallel flow. We need not write out the tendency operator as an explicit matrix: the Arnoldi (Lehoucq et al. 1998) algorithm can compute the eigenvectors and eigenvalues of a sparse linear operator that is specified as an algorithm like that described in the previous paragraph. In addition, the Arnoldi technique can solve for a *small number* of eigenvalues of desired characteristics, rather than finding the entire eigenspectrum. Since coupled modes that are rapidly damped will not be observable in nature, we solve for the eigenvalues with the most positive real part.

REFERENCES

Andersson, P., M. Berggren, and D. S. Henningson, 1999: Optimal disturbances and bypass transition in boundary layers. *Phys. Fluids,* **11,** 134–150.

Barnston, A., and R. E. Livezey, 1987: Classification, seasonality and persistence of low-frequency circulation patterns. *Mon. Wea. Rev.,* **115,** 1083–1126.

Barsugli, J. J., and D. S. Battisti, 1998: The basic effects of atmosphere–ocean thermal coupling on middle-latitude variability. *J. Atmos. Sci.,* **55,** 477–493.

Bretherton, C., and D. Battisti, 2000: An interpretation of the results from atmospheric general circulation models forced by the time history of the observed sea surface temperature distribution. *Geophys. Res. Lett.,* **27,** 767–770.

Cayan, D., 1992: Latent and sensible heat flux anomalies over the northern oceans: The connection to monthly atmospheric circulation. *J. Climate,* **5,** 354–369.

Cessi, P., 2000: Thermal feedback on windstress as a contributing cause of climate variability. *J. Climate,* **13,** 232–244.

Czaja, A., and C. Frankignoul, 1999: Influence of the North Atlantic SST on the atmospheric circulation. *Geophys. Res. Lett.,* **26,** 2969–2972.

——, and J. Marshall, 2001: Observations of atmosphere–ocean coupling in the North Atlantic. *Quart. J. Roy. Meteor. Soc.,* **127,** 1893–1916.

Deser, C., and M. Blackmon, 1993: Surface climate variations over the North Atlantic ocean during winter: 1900–1989. *J. Climate,* **6,** 1743–1753.

Farrell, B. F., 1982: The initial growth of disturbances in a baroclinic flow. *J. Atmos. Sci.,* **39,** 1663–1686.

——, 1989: Optimal excitation of baroclinic waves. *J. Atmos. Sci.,* **46,** 1193–1206.

Ferreira, D., C. Frankignoul, and J. Marshall, 2001: Coupled ocean–atmosphere dynamics in a simple midlatitude climate model. *J. Climate,* **14,** 3704–3723.

Frankignoul, C., and K. Hasselman, 1977: Stochastic climate models. Part II: Application to sea surface temperature variability and thermocline variability. *Tellus,* **29,** 284–305.

——, P. Müller, and E. Zorita, 1997: A simple model of the decadal response of the ocean to stochastic wind forcing. *J. Phys. Oceanogr.,* **27,** 1533–1546.

Gallego, B., and P. Cessi, 2000: Exchange of heat and momentum between the atmosphere and ocean: A minimal model of decadal oscillations. *Climate Dyn.,* **16,** 479–489.

Goodman, J., and J. Marshall, 1999: A model of decadal midlatitude atmosphere–ocean coupled modes. *J. Climate,* **12,** 621–641.

——, and ——, 2002: Using neutral singular vectors to study low-frequency atmospheric variability. *J. Atmos. Sci.,,* **59,** 3206–3222.

Hasselmann, K., 1988: PIPs and POPs: The reduction of complex dynamical systems using principal interaction and oscillation patterns. *J. Geophys. Res.,* **83** (D9), 11 015–11 021.

Hurrell, J. W., and H. van Loon, 1997: Decadal variations in climate associated with the North Atlantic oscillation. *Climatic Change,* **36,** 301–326.

Jin, F.-F., 1997: A theory of interdecadal climate variability of the North Pacific ocean–atmosphere system. *J. Climate,* **10,** 324–338.

Kushnir, Y., 1994: Interdecadal variations in North Atlantic sea surface temperature and associated atmospheric conditions. *J. Climate,* **7,** 141–157.

Lehoucq, R., D. Sorensen, and C. Yang, 1998: ARPACK Users' Guide: Solution of Large-Scale Eigenvalue Problems with Implicitly Restarted Arnoldi Methods. SIAM Publications, 140 pp.

Luchini, P., 2000: Reynolds-number-independent instability of the boundary layer over a flat surface: Optimal perturbations. *J. Fluid Mech.,* **404,** 289–309.

Marotzke, J., R. Giering, K. Q. Zang, D. Stammer, and T. Lee, 1999: Construction of the adjoint MIT ocean general circulation model and application to Atlantic heat transport sensitivity. *J. Geophys. Res.,* **104** (C12), 29 529–29 547.

Marshall, J., and F. Molteni, 1993: Toward a dynamical understanding of planetary-scale flow regimes. *J. Atmos. Sci.,* **50,** 1792–1818.

——, H. Johnson, and J. Goodman, 2001: A study of the interaction of the North Atlantic Oscillation with ocean circulation. *J. Climate,* **14,** 1399–1421.

Mehta, V. M., M. J. Suarez, J. V. Manganello, and T. L. Delworth, 2000: Oceanic influence on the North Atlantic Oscillation and associated Northern Hemisphere climate variations: 1959–1993. *Geophys. Res. Lett.,* **27,** 121–124.

Molteni, F., and T. Palmer, 1993: Predictability and finite-time instability of the northern winter circulation. *Quart. J. Roy. Meteor. Soc.,* **119,** 269–298.

Navarra, A., 1993: A new set of orthonormal modes for linearized meteorological problems. *J. Atmos. Sci.,* **50,** 2569–2583.

Neelin, J. D., and W. Weng, 1999: Analytical prototypes for ocean–atmosphere interaction at midlatitudes. Part I: Coupled feedbacks as a sea surface temperature dependent stochastic process. *J. Climate,* **12,** 697–721.

Rodwell, M. J., D. P. Rowell, and C. K. Folland, 1999: Oceanic forcing of the wintertime North Atlantic oscillation and European climate. *Nature,* **398,** 320–323.

Stommel, H., 1948: The westward intensification of wind-driven ocean currents. *EOS, Trans. Amer. Geophys. Union,* **99,** 202–206.

Sutton, R. T., and M. R. Allen, 1997: Decadal predictability of North Atlantic sea surface temperature and climate. *Nature,* **338,** 563–566.

Wallace, J. M., and D. S. Gutzler, 1981: Teleconnections in the geopotential height field during the Northern Hemisphere winter. *Mon. Wea. Rev.,* **109,** 784–812.

Watanabe, M., and M. Kimoto, 2000: Ocean atmosphere thermal coupling in the North Atlantic: A positive feedback. *Quart. J. Roy. Meteor. Soc.,* **126,** 3343–3369.

Weng, W., and J. D. Neelin, 1998: On the role of ocean–atmosphere interaction in midlatitude interdecadal variability. *Geophys. Res. Lett.,* **25,** 167–170.